A New Wide-Field Corrector for the Kitt Peak Mayall 4-m Telescope

George H. Jacoby, Ming Liang, David Vaughnn, Rich Reed, and Taft Armandroff
National Optical Astronomy Observatories (NOAO)[a]
P.O. Box 26732, Tucson, Arizona, 85726-6732

ABSTRACT

The Kitt Peak Mayall 4-m telescope required a new prime focus corrector having a flat focal plane covering 36 arcmin on a side (51 arcmin diagonal) to accommodate the Mosaic 8K x 8K CCD system. The scientific requirements for the new corrector included atmospheric dispersion compensation (ADC), excellent near-UV efficiency, excellent image quality, and extremely low scattered light and ghosting. The optical system designed to meet these demands exhibits excellent and stable performance through its first year of operation. This paper describes the innovative design and engineering aspects of the corrector. Science verification data are presented to demonstrate some of the attributes of the new corrector.

Keywords: optical design, corrector, atmospheric dispersion compensation, astronomical imaging, CCD Mosaic, AR coatings

1. INTRODUCTION

For 25 years, the original doublet and triplet correctors[1] for the Mayall 4-m (f/2.8) telescope on Kitt Peak have served the needs of photographic and modest-field CCD imaging. With the very wide fields attainable with mosaics of large-format CCD systems, though, the existing correctors cannot deliver the desired optical performance. This paper describes the 4-m prime focus corrector (4mPFC), a new four-element corrector that has been built specifically for wide-field optical imaging. In particular, we describe the motivation for building the corrector, its design philosophies and trade-offs, and its design implementation schemes. We also review the performance of the new corrector during its first year of science operations.

1.1. Motivation for building a new corrector

The fused-silica doublet that had been used extensively with simple CCD systems provided a field-of-view of 16'x16', but the image quality at the field edge was poor. The unvignetted field falls more than a factor of 2 short of the entire field of the NOAO 8K X 8K Mosaic (36'x36') and the doublet clearly is not usable with this new instrument. The blue and red triplets (UBK7 and BK7) and offer a 40' field suitable for 5-6 inch plates. However, their design suffers in a variety of other ways.

1. The corners of the CCD Mosaic field are vignetted (Mosaic's diagonal field-of-view is 51'; or 6.8 inches).
2. The triplet design assumes that there is little glass between the rear corrector element and the detector, whereas the CCD Mosaic requires a 16 mm thick dewar window and 12 mm thick filters. With the triplet, the added glass causes severe off-axis aberrations, degrading the delivered image quality (DIQ) to several arcsec.
3. The ultraviolet (UV) efficiency of the triplets is poor at the blue end of the photometric U-band. Since many imaging programs at Kitt Peak already require long exposures in this bandpass, further inefficiencies severely impact the effectiveness of the telescope.
4. Kitt Peak has made major upgrades to the 4-m telescope image performance. It is expected that the DIQ frequently will be under 0.8". To achieve this degree of image quality demands that atmospheric dispersion be compensated up to 70° zenith distance, especially in the U and B bands (Figure 1), and that the corrector system be capable of alignment. Neither of these requirements could be met with the existing triplets.

1.2. Design requirements

At a minimum, the 4mPFC must present an unvignetted field-of-view to the Mosaic CCD camera, which is defined by Muller et al.[2] as 123.9 x 125.9 mm, or 176.6 mm on the diagonal (51'). Since this field is delivered to an electronic detector system

[a] Operated by the Association of Universities for Research in Astronomy, Inc. (AURA) under cooperative agreement with the National Science Foundation.

consisting or 8 CCDs, the focal plane must be flat across the entire imaging area; otherwise, the point-spread-function (PSF) will vary due to focus changes. Furthermore, the PSF must not vary across the field due to aberrations that might degrade the images by more than 10% when the telescope primary and atmosphere deliver images as good as 0.5". Figure 1 shows that this last constraint demands an atmospheric dispersion compensation (ADC) system.

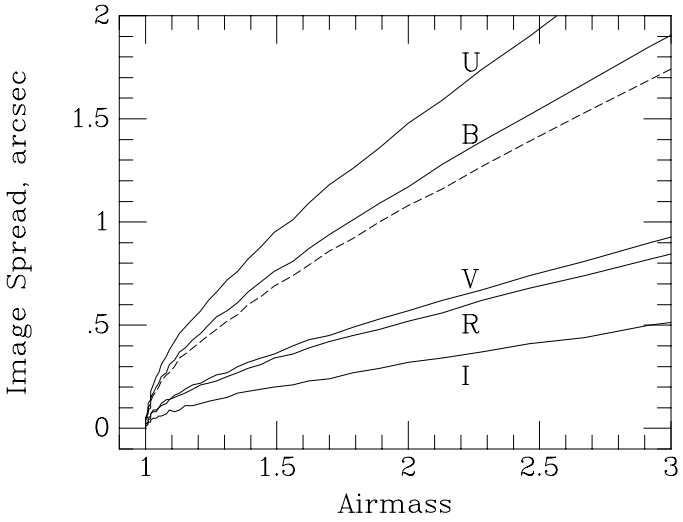

Figure 1. The effect of the atmosphere on the image spread for the 5 major passbands (UBVRI) as a function of airmass. "Image spread" is defined as the difference in position of a star on the sky due to differential atmospheric refraction at the edges (half power points) of each filter. In actual observing situations, the true U-band effect (indicated by the dashed line) is reduced due to atmospheric absorption and poor detector response for light bluer than ~340 nm.

The total optical efficiency of the corrector and its image quality was required to be excellent across the entire optical region, from the atmospheric cutoff at 320 nm to the near-infrared at 1000 nm. Performance, though, was optimized for the spectral region defined by the BVR bandpasses (390 - 720 nm). Given the requirement for an ADC, which severely limits the choice of glasses (see below), combined with the requirements for low internal reflections and ghosting, which implies excellent coatings, some compromise in efficiency is necessary.

Because of the wide-field nature of the imager, bright stars will always be present in or near the imaged field. Control of scattered light forced us to pay special attention to coatings. In addition, any mechanical part that might see the sky was blackened or flocked to reduce reflections within the corrector. Also, any cement between elements was reviewed for its scattering properties (see Section 2.4).

The design also included operational requirements. First, the 4mPFC must be used with the existing CCD imager, the 4-m prime focus CCD (PFCCD), so that the corrector would not need to be swapped when observations were being made without the Mosaic. This issue addresses both safety and operational costs and offers superior optical performance with PFCCD. From a design standpoint, two conditions are imposed. First, the backfocal distance of the corrector must be sufficient to accommodate the longer throw of the PFCCD. Second, the image quality must be maintained through a path length of glass through filters and dewar windows that is 16 mm less than with the CCD Mosaic. Fortunately, this can be achieved due to the much smaller field-of-view of PFCCD.

In addition, the 4mPFC must maintain focus through the different filters when they are constructed to be parfocal, even during rotation of the ADC prisms. Telescope focus, however, is controlled by moving the entire corrector-plus-imager group.

Finally, there are requirements related to the instrument environment, servicing, safety, and life expectancy. The optical performance of the instrument must remain within specification over the operation temperature range which is -17 C to 27 C. The performance must remain within specification over a range of zenith distances (angles from zenith) which we adopt as 0° to 70°. The minimum lifetime of the instrument is ten years. Degradation due to foreign and internally dissociated contaminations must not jeopardize performance.

1.3. Preliminary design options and trade-offs

A design for the CTIO Blanco 4-m telescope provided a good starting point to consider. That telescope recently received a new corrector designed by Richard Bingham[3] with scientific requirements similar to, but different in detail from, those listed above. The KPNO corrector was intended for imaging, whereas the CTIO corrector was designed with an emphasis on multi-fiber spectroscopy. The consequent differences between the two designs centers on the ADC -- the 4mPFC ADC components have only ADC functions (see Figure 2).

This point is reflected in the philosophy of how the ADC functions: the CTIO corrector was required to provide atmospheric compensation across a very broad wavelength region; the KPNO corrector only provides correction across the relatively narrow region of a filter bandpass, typically 100 nm. This latter approach yields slightly better imaging over a restricted wavelength region at any one time. Also, the 4mPFC is not achromatized and is not intended to cover an unfiltered

wavelength range. Longitudinal chromatic aberration is present, but the use of low-dispersion SiO_2 keeps this manageable within a given band. There is, however, a band-to-band change in focal length (i.e., the plate scale increases by 0.1% from the U to the I band).

Figure 3 shows that the glasses used in the KPNO ADC (UBK7 and LLF6) provide good UV transmission. Furthermore, the flat ADC surfaces reduce the complexity of the KPNO ADC, and its location in the light path reduces the overall size, weight, and cost.

Table 1 summarizes the optical prescription for the 4mPFC design. Although the CTIO corrector has fewer elements, they are more complex to build and to maintain alignment because ADC functions are incorporated into power elements having wedged, curved surfaces.

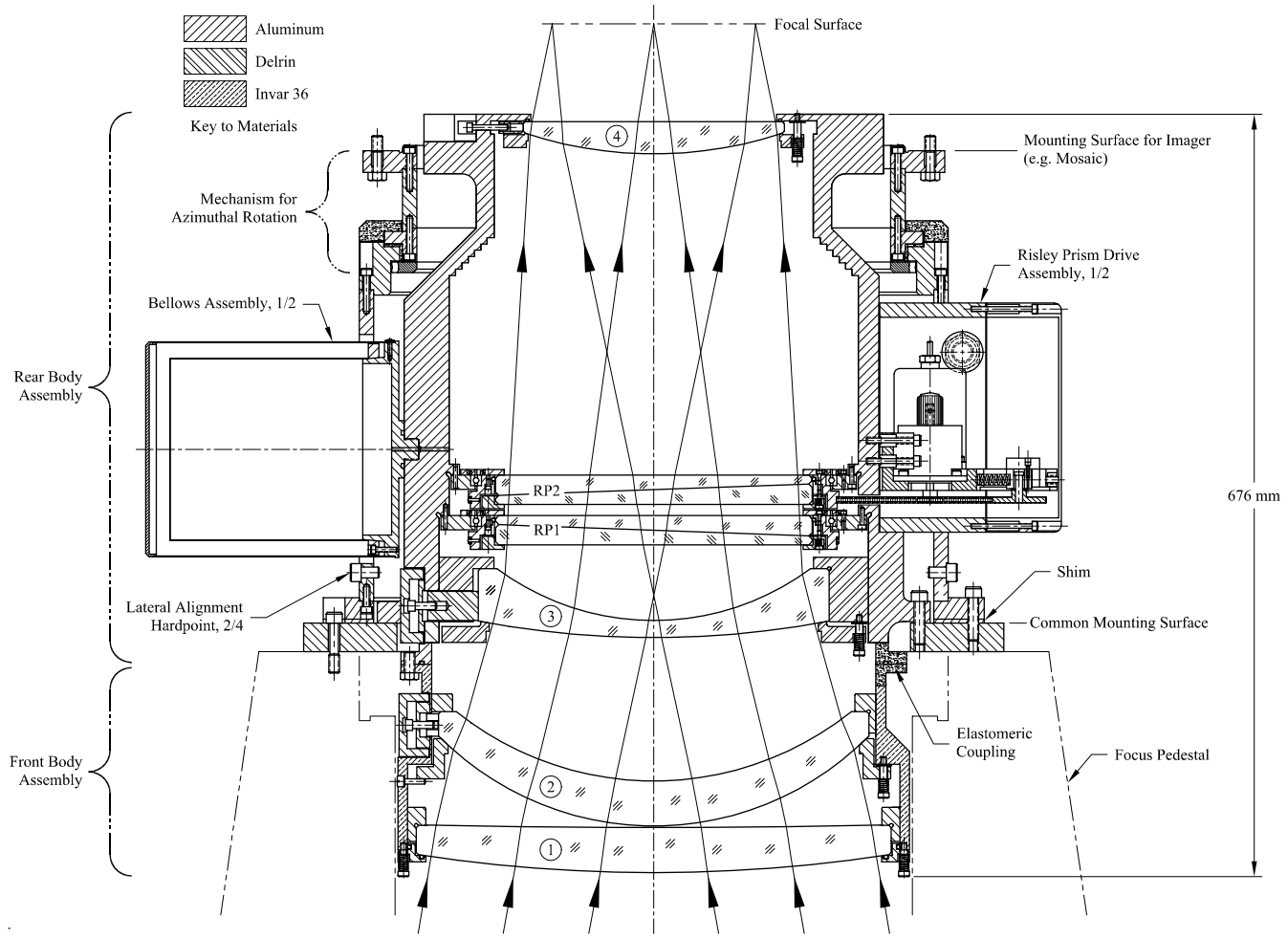

Figure 2. The opto-mechanical assembly for the new 4-m prime focus corrector. Elements #1, #2, #3, and #4 are SiO_2. The ADC materials comprising RP1 and RP2 are UBK7 (rear) and LLF6 (front), where "rear" is closer to the detector.

In considering the choice of the two glasses for the ADC prisms, there were four drivers.

1. Both glasses should have high UV transparency.
2. The refractive indices at the central wavelength should be similar.
3. The dispersions must be different.
4. The bulk size must be available.

Three pairs of glasses were considered: UBK7-LLF6, PSK3-LLF1 and Ultran30-LLF2. The Ultran30-LLF2 pair has the best UV transparency, while PSK3-LLF1 is the poorest. Also, the Ultran30-LLF2 and PSK3-LLF1 pairs have similar indices at the central wavelength, but UBK7-LLF6 does not. The best choice is Utran30-LLF2, but it is very difficult to obtain sufficiently large Ultran30 glass. Thus, we chose the UBK7-LLF6. Since the central refractive indices of this glass pair differ, the outer surfaces of the Risley-prisms were made non-parallel.

Table 1, Optical Prescription for the 4mPFC

Location/Surface	Radius	Following The Surface		DIA
		Thickness	Material	
Bottom of the Secondary (Obscuration)	-	7976 mm	-	1968 mm
Primary Mirror (Focus→ Focus Varies)[1]	21336 mm	9976.9 mm	Reflection	4000 mm
Lens #1	1379.88 mm	39.80 mm	SiO_2	419.86 mm
	8483.60 mm	1.50 mm	-	400.00 mm
Lens #2	266.76 mm	39.85 mm	SiO_2	380.36 mm
	278.89 mm	127.14 mm	-	349.32 mm
Lens #3	828.42 mm	15.08 mm	SiO_2	310.40 mm
	231.97 mm	66.18 mm	-	277.08 mm
Risley Prism Element #1A[2]	-	12.59 mm	LLF6	280.08 mm
Risley Prism Element #1B[3]	-	12.98 mm	UBK7	280.08 mm
	-	9.39 mm	-	280.08 mm
Risley Prism Element #2A[4]	-	13.50 mm	LLF6	280.08 mm
Risley Prism Element #2B[5]	-	13.11 mm	UBK7	280.08 mm
	-	285.80 mm	-	280.08 mm
Lens #4	362.67 mm	28.60 mm	SiO_2	230.82 mm
	-	44.60 mm	-	230.82 mm
Typical Filter (Mosaic)	-	12.0 mm	Varies	206.5 mm
	-	11.83 mm	-	206.5 mm
Dewar Window (Mosaic)	-	15.38 mm	SiO_2	224 mm
	-	11.80 mm	Vacuum	224 mm
Focal Surface (Mosaic)	-	-	-	176.6 mm

[1]Conic Constant is -1.09763, Clear Aperture is 3760 mm
[2]Angle wrt optical axis is .076°, Set for Null-Dispersion
[3]Angle wrt optical axis is 2.100°, Set for Null-Dispersion
[4]Angle wrt optical axis is -.074°, Set for Null-Dispersion
[5]Angle wrt optical axis is -2.233°, Set for Null-Dispersion

2. DESIGN PHILOSOPHY AND IMPLEMENTATION

2.1. Build-to-print approach

One of our goals was to complete the project within two years to be ready for use with the Mosaic. Until recently, NOAO's complex optical instrumentation passed through an extended and iterative period of optical assembly, alignment, testing, and verification. Null-tests must be designed, fabricated, and executed. Because of our schedule, this approach was prohibitive.

Instead, we adopted a deterministic "build-to-print" approach. In-house experience with this deterministic approach was limited and consequently, presented a high risk. We decided to employ the build-to-print philosophy first to the wide-field Mosaic corrector for the 0.9-m Cassegrain telescope, a relatively simple 2-element SiO_2 system that is currently in service. This corrector was finished, tested in-situ, and verified to function as advertised before the commitment was made to complete the design and begin fabrication of the 4mPFC according to similar principles.

The main tenet of the build-to-print approach is a careful tolerance analysis and distribution of allowable departures from a theoretically perfect opto-mechanical system. A simple model is constructed where each contribution to the overall (measured) imagery is calculated (Figure 4). The horizontal line marked **Raw Seeing** represents 0.5 arcsec seeing in units of linear scale at the focal surface. The horizontal line above this represents the first scientific requirement. The field radius of 0.42° corresponds to the corner of the Mosaic array. The line marked **Diffraction** is the Airy disk diameter. The field-dependent aberrations represent a theoretically perfect implementation of the optical model and are computed for the astronomical V band (490 - 610 nm).

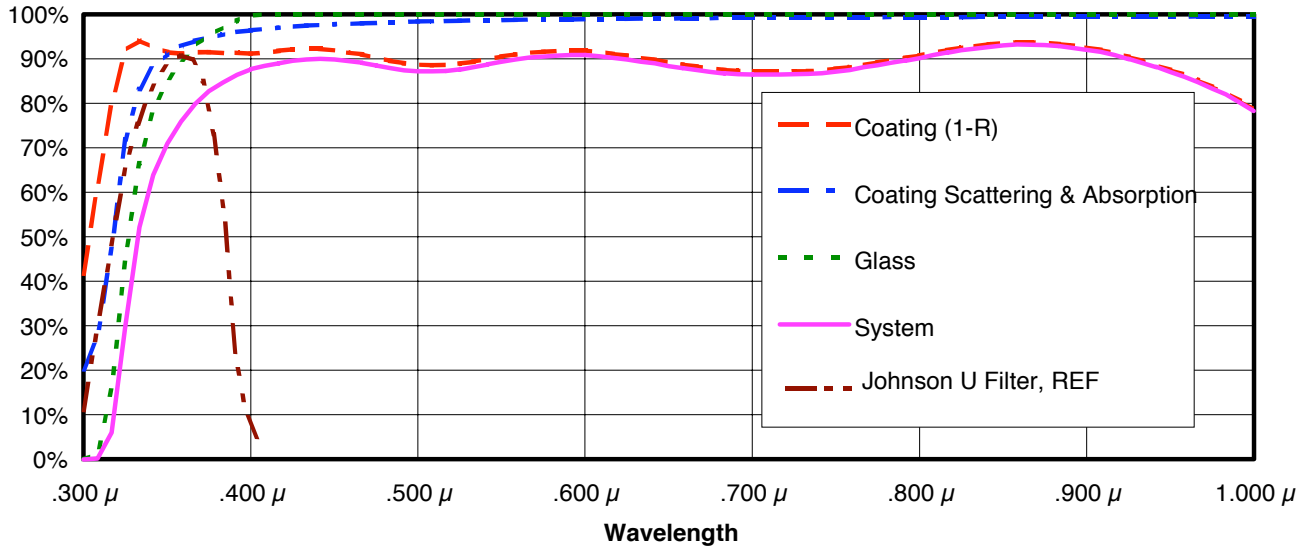

Figure 3. The transmissive efficiencies of the KPNO corrector and the factors entering the total performance. The transmission curve for the Johnson U-band filter also is shown. It was a very high priority that the KPNO corrector work well in this UV region.

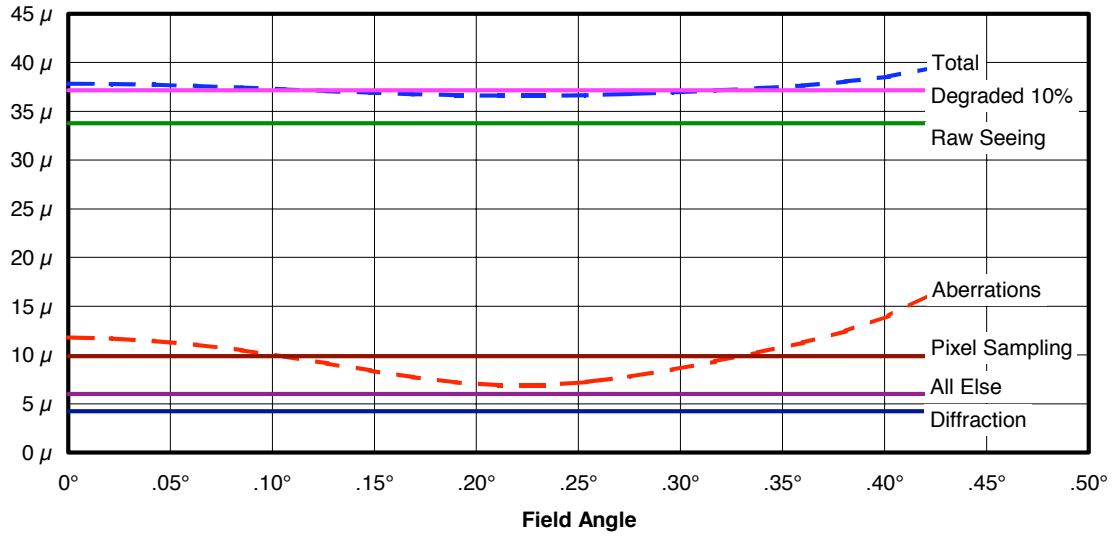

Figure 4. The corrector error budget (RMS full-width) as a function of position in the field-of-view. One arcsecond corresponds to 57μm. The Raw Seeing RMS of 34 μm (0.6") approximately represents the non-Gaussian seeing disk having FWHM = 0.5".

The line marked **All Else** represents the allowable degradation due to fabricating, assembling, aligning, and mechanically mounting real optics. The last requirement covers flexural, thermal, and long-term mechanical creep. **All Else** includes

compensated chromatic aberration due to differential atmospheric refraction. There are 6 μm of available RMS full-width degradation which is distributed among these effects. The line marked **Total** is the quadrature sum of all contributions.

The lathe assembly[4] technique was employed together with a careful analysis and quality control of the optical fabrication. Each optical surface is referenced to, and measured with respect to, two registration surfaces, such as an annulus (axial) and outside diameter (radial). The runout (measurable misalignment) for each optical surface was toleranced and verified to meet specification. Also, a design was adopted whereby all mating mechanical mounting surfaces could be machined from "one side". The entire system was fabricated with extra material on the mating surfaces and assembled together.

After all of the optical elements were fabricated, the system was re-optimized to determine final spacings. Then each mechanical mounting surface and the surface which mates to a common mounting surface with the Mosaic imager were machined in a single lathe assembly operation. This reduces the misalignment of each surface to no more than 40 - 60 μm (12 μm for the runout of the lathe and 25 - 50 μm for the optical fabrication).

2.2. Opto-mechanical issues

In general, each optical element is held quasi-kinematically, preloaded with three times its weight in both the radial and axial directions against mechanical mating surfaces. In the radial direction, each element is preloaded quasi-kinematically against two pads spaced 120° away from the radial preload and each other. Prior to the lathe assembly operation, an additional dummy pad is installed opposite one of the two radial locating pads for each element. This allows a precision measurement across the diameter to perfectly match the measured diameters of the optics. The axial preload for element #4 was increased to over three times its weight to overcome the restoring force of an o-ring seal.

The most accurate opto-mechanical mount can be rendered pointless and dangerous by changes in temperature. There are two kinds of thermal induced aberrations -- those resulting from axial and radial misalignments of the optics.

For two reasons, axial changes can be neglected. First, while the operating temperature range is relatively large (34 C), there is much less change within a given night (~4 C). The primary effect of axial displacements (< 100 μm front-to-rear) is focus change. Focus is set at least once a night and usually checked if the ambient temperature changes more than ~1-2 C. Spacing of some of the optical elements (e.g., #1 and #2) is much more critical than ±50 μm. Because of their proximity, though, their axial positions change very little. However, one important provision is made. The axial locating surfaces are machined at the temperature of our instrument shop, ~23 C. The average nighttime temperature on Kitt Peak is 10 C. The relative position of each axial mounting surface was calculated so that when cooled 13 C, the optical separations would be optimum.

Radial misalignments are more serious. We chose to avoid a complex tolerancing problem and eliminated asymmetrical contributions to the error budget by athermalizing the radial locations of the optical elements. This was accomplished via a judicious choice of two materials with dissimilar coefficients of thermal expansion. Fused silica has a very low coefficient of thermal expansion, α_{LENS}. A pad material is chosen with a larger coefficient of expansion, α_{PAD}, than the accompanying cell (structure) material, α_{CELL}. The interface diameter between the pad and cell, D_{INT}, is calculated so the expansion of the pad and cell perfectly match that of the optical element[5].

$$D_{INT} = D_{LENS} \frac{\alpha_{PAD} - \alpha_{LENS}}{\alpha_{PAD} - \alpha_{CELL}} \qquad [1]$$

The two materials must be selected for long-term stability, outgassing properties, and good thermal match. Without a good match, the radial pad thickness becomes impractically small or cumbersomely large. The best match was identified as acetal resin (Delrin®) for the pad and 6061 aluminum for the cell. Advantages to this combination include availability, ease of machining, and ease of finish (none needed for black Delrin). This combination was adopted for the large rear body assembly. The front portion of the 4mPFC was limited by available diametrical clearance in the prime focus cage and precluded this combination. Here, the best combination was 6061 aluminum with invar (see Figure 2). Thermal-induced stress in the interface between the front and rear body cells was reduced by slotting the mating flanges in 12 places to allow small symmetrical radial flexure. The gaps in the slots were filled with an opaque elastomer.

Independent verification of the coefficient of expansion for the three materials was made. Long (50 mm) test witness samples were fabricated from the same stock as used for the employed parts and were subjected to the same metallurgical operations (Table 2). A large solid billet of 6061 aluminum was procured for the rear body assembly cell. The rest of the aluminum parts were made from a single 6061-T6 plate. Both the 6061 and invar cell materials changed significantly during heat treatment. The measurement for Delrin was 15% higher than the catalog value. This shifted the location of the interface diameter at element #3 inward by over 10 mm, bringing it to within 1 mm of the previously roughed out dimension.

Table 2. Measurements of Thermal Expansion Coefficients

Thermal Expansion	SiO_2	Delrin	6061 Billet	6061 Parts	Invar 36 FM
Catalog	52.2E-8 /°C	1.12E-4 /°C	23.2E-6 /°C	23.2E-6 /°C	1.26E-6 /°C
Measured Stock		1.29E-4 /°C	23.0E-6 /°C	23.0E-6 /°C	
After Heat Treatment			23.8E-6 /°C		1.31E-6 /°C
After Stress Relief			23.9E-6 /°C		1.34E-6 /°C

The radial mounting for element #1 is a special case. Utilizing the combination of an Invar cell with aluminum pads provides enough room for an athermalized mount but not enough for a radial preload mechanism. Instead, a hard mounting technique[6] was used. The radial location of the lens is constrained by machining the inner diameter of the pads with very small clearance to the lens. The diametrical gap is determined by the science-driven performance requirement. Having the lens radially misaligned by a small offset causes two effects: a first-order prismatic steering of the beam, and field dependent aberrations, with the effect of the former being greater. If a long exposure is made starting on one side of zenith and is tracked through zenith, the lens can shift from one side of the gap to the other. This creates a double exposure with a separation dependent upon the gap size, power of the lens, and system focal length.

In this case, we felt that the maximum allowable angular separation was 0.05 arcseconds on the sky. This corresponds to a linear change of 3 μm at the focal surface and an allowable diametrical gap width of 15 μm. This is extremely difficult to machine and to assemble. A temperature-compensated gage system was developed to transfer the diameter of the lens to the bore diameter during lathe assembly. The tolerance on the bore diameter was +5/-3 μm. During assembly, the angular alignment of the lens had to be kept within 0.08° of the finished bore to prevent jamming. In addition, there is no access around the 420 mm diameter, 10 kg element to support it during assembly. A special vacuum fixture was designed and fabricated to allow it to be lowered vertically into position.

2.3. The ADC

While lateral positioning of the Risley prisms is much less critical than the other optical elements, angular alignment with respect to the optical axis is important (see Figure 5). Each prism element is unique (wedge angle) as is each Risley prism. However, the rear (UBK7) surface of each prism is oriented perpendicular to the system optical axis. This surface is registered to an accurate mounting surface machined during lathe assembly by an axial preload ring. Each prism is held radially via an o-ring to allow for differential thermal expansion.

Each ADC drive mechanism utilizes sprockets, a preloaded chain, a stepper motor, and encoder. The prisms can be freely rotated in both directions indefinitely and there are 16 revolutions of both the motor and encoder per prism rotation. The stepper motor has 200 full-steps per rotation; hence each full-step rotates the Risley prism 0.11°. The motor is operated in full-step mode so that there is no movement when the motor is de-energized. The encoder resolution is significantly greater than a full-step. The encoders incorporate low-power internal electronics to achieve absolute encoding. The internal battery allows un-powered non-volatile operation for more than a month. When power is not applied for an extended period, or when chosen by the user, the drive mechanisms can be re-indexed. A limit switch is precisely placed to coincide with the null-dispersion condition. Re-indexing moves each Risley prism to the null position and recalibrates the absolute encoders.

2.4. Stray light

Considerable effort was made to reduce stray light. The first step was the design of the opto-mechanical geometry. There are no grazing incidence surfaces within the 4mPFC. Additionally, the entire instrument is light-tight. The ADC drive encoders utilize internal LEDs. These encoders are completely baffled from the light path.

All surfaces were blackened if they directly adjoin the optical path or if they are within the field-of-view of the direct surfaces (secondary scattering). Black Delrin stock was used. All aluminum parts were black anodized. A special flat black coating (Lord Aeroglaze Z306) was applied to the internal Invar cell and the fasteners within view of the primary mirror. The elastomer which was used to seal gaps and holes through the structure (Dow Corning® 93-500) was made black and opaque by the addition of 15% black xerographic toner (carbon black) by volume. Finally, the very front of the 4mPFC (the stainless steel axial clamp ring for element #1) was flocked to lower its bidirectional reflectance distribution function (BRDF)[7].

Choosing good very broad wavelength anti-reflection (A/R) coatings for all the optical elements is doubly important to the delivered signal-to-noise ratio of the images. Higher transmission improves the signal while lower specular reflection, coating absorption, and scattering all diminish stray light. A proprietary coating developed at Continental Optical Corp. (Hauppage, NY) for SiO_2 was optimized for the wavelength region of 330 - 1000 nm. This was applied to 7 of the 8 optical surfaces. The coating was modified for use with the two ADC glass types (4 surfaces). The front surface of the last SiO_2 optical element (element #4A) was coated with a Sol-Gel coating at Cleveland Crystals, Inc. (Highland Heights, OH). Although this coating has higher reflectance at the ends of our spectral range, it has very good performance in the region where most narrow-band interference filters are used, reducing the intensity of a ghost pupil image (see Section 4). Figure 6 illustrates the measurements of these three A/R coating types.

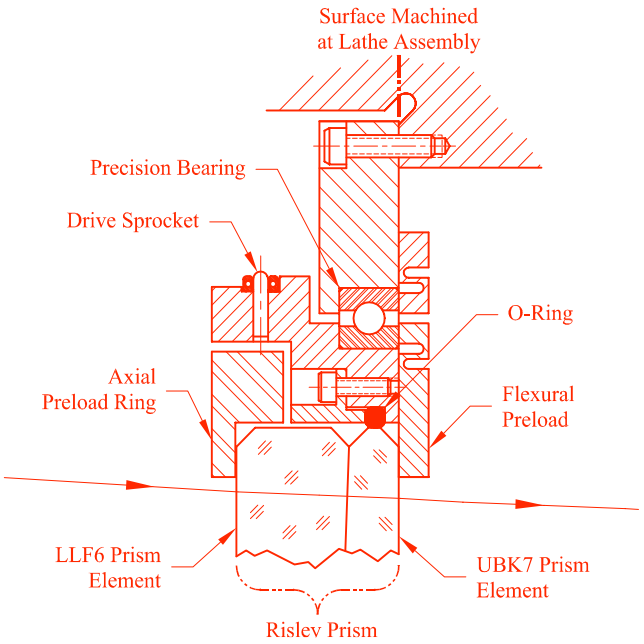

Figure 5. The opto-mechanical layout of the ADC prisms.

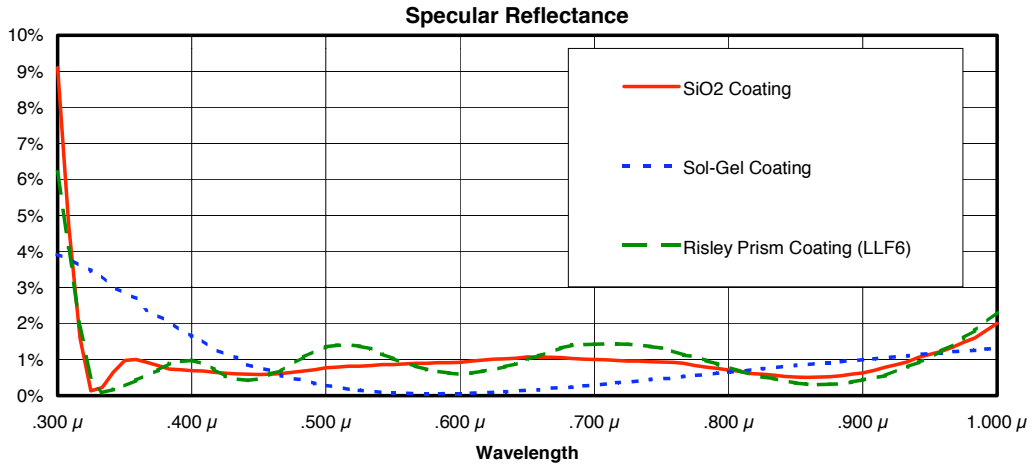

Figure 6. The reflectance exhibited by the three different coatings used in the 4mPFC. The Sol-Gel has extremely low reflectance (0.1-0.2%) in the center of the optical region where most narrow-band imaging is done. The amplitude of the ghost pupil increases in direct proportion to the reflectance of this coating.

Ghost images are highly undesirable for astronomical imaging. These are formed by specular reflections from surfaces nominally transmissive or absorptive. It is possible to have ghost images of both objects and pupils. Object ghosts are double reflections from close surfaces, and narcissus where the first stray reflection is off the focal surface. Pupil ghosts can be formed by mechanical stops and apertures. In both cases, coatings and optimization of surface geometry can spread out and reduce the amplitudes of ghost images to an acceptable level.

A scientific requirement was that the intensity of the disc of stray ghost light around each star be dominated by the ghost image formed from a reflection of a scientific-grade CCD and the inside surface of the dewar window. This meant the next largest contribution be limited so that the ratio of intensities of light within the disk of ghost light, I_G, to the integrated light within the image core be $<10^{-8}$. For two adjacent plane parallel plates, this can be estimated by the reflectance of the two surfaces, R, the separation of the plates, SEP, the f/ratio of the imaging system, f/# (3.14 for the Mayall 4-m), and the image size, D_I. Equations 2-4 show how the separation between the Risley prisms was determined to be 10 mm. This same phenomenon motivates a thick dewar window (12 mm for the Mosaic imager).

$$\frac{I_G}{I_I} = R^2 \left(\frac{D_I}{SEP/f/\#} \right)^2 \qquad [2]$$

$$= 1\%^2 \left(\frac{.038\,mm}{10\,mm/3.14} \right)^2 \qquad [3]$$

$$= .4 \times 10^{-8} \qquad [4]$$

The final item relating to stray light again concerns the ADC. Because of the large diameter of the Risley prisms (280 mm), the goal to preserve good transmitted wavefront through the ADC over the extended temperature range, and the requirement to be transmissive in the U band, a choice was made to utilize a relatively thick layer (0.18 mm) of Dow Corning® SYLGARD 184, a flexible adhesive, to cement the prism elements,. This is a two-part elastomeric encapsulant. During testing of this product, though, it was found that per unit volume, it produces significantly more scattering than normal optical adhesives because there are colloidally suspended particles in the base supplied by the manufacturer. These sub-micron particulates act as scattering centers to increase stray light, but can be removed by a progressive filtration process. The adopted sequence was to use filters of 1.0 μm followed by .5 μm and then .2 μm. The material was processed through each stage twice. We estimate that this reduced the total integrated scatter by a factor of ~20 at 633 nm, improving it to a level typical of normal optical adhesives.

2.5. Longevity

Measures were taken to ensure that performance of the 4mPFC lasts for the intended lifetime with little maintenance. Both front and rear cell bodies were heat treated to produce a stable matrix. The Invar 36 FM front cell was procured as a heat treated forging (30 min at 829 C W/Q). This was then machined very carefully so that the coefficient of thermal expansion was not affected. It was further stress relieved (90 min at 315 C St/A/C + 48 hr at 96 C A/C) prior to lathe assembly. The 6061 aluminum rear cell body was procured as a billet in the T0 temper. It was rough machined and heat treated to the T6 condition (75 min at 529 C W/Q + 8 hr at 177 C). After machining, it also was stress relieved (2 hr at 218 C A/C) prior to lathe assembly. [Note: W/Q=water quenched; A/C=air cooled; St/A/C=still air cooled.]

We chose to isolate the internal workings of the instrument from the environment by making the structure hermetically sealed and filled with clean dry N_2 gas. Materials internal to the 4mPFC were chosen to have low-outgassing properties. Teflon was used for electrical wire insulation and cable clamps. The gasket material (Rogers PORON® 4701-01), elastomeric encapsulant (Dow Corning® 93-500), and black coating (Lord Aeroglaze Z306) are all low-outgassing products developed for space use.

A bladder system was implemented to allow the instrument to track changes in local pressure. The internal gas volume of the instrument is ~48 *l*. A P-V temperature range of 34 C requires an available volume of about 11%, or 5.6 *l*. An additional 3% volumetric change, 1.4 *l*, is needed for uncorrelated barometric pressure. Two bladders were designed with a capacity of 6.6 *l*, yielding 10% more than the 6.0 *l* needed. There is a cracking valve to bleed-off purging N_2 gas or any time the internal pressure becomes slightly above ambient. Purging is done through a one-way valve and 5 - 10 μm filter.

3. ON-SKY TESTING AND PERFORMANCE

The optical performance of the corrector is much better than typical observing conditions can challenge. That is, unless the atmospheric stability and telescope/dome environment are excellent, seeing dwarfs the aberrations from the corrector. Consequently, on-sky testing during those rare moments of superb conditions has been very limited.

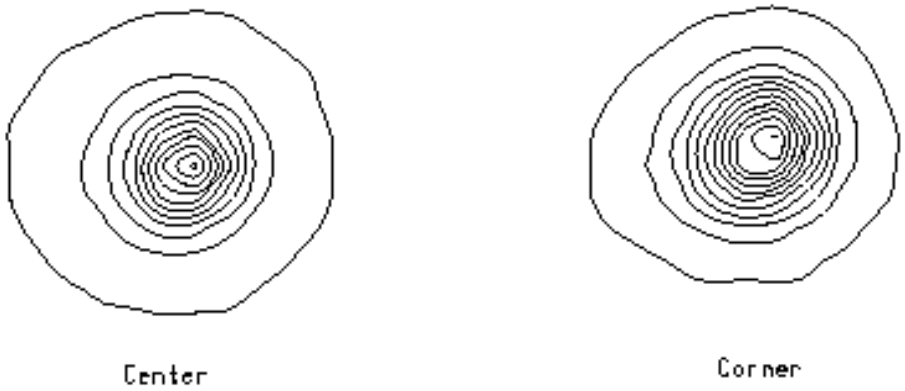

Figure 7. The two contour diagrams are from a star (left) near the center of the 4-m CCD Mosaic and from a second star (right) near an extreme corner at a radial distance of 23'. The central image has a FWHM of 2.5 pixels (0.65"); the corner star has a FWHM of 3.1 pixels (0.76"). A contour represents a 10% step along the intensity profile of the star; the outermost contours extend over 10 pixels. This R-band image, at a zenith distance of 10° (airmass of 1.01), did not use the ADC.

3.1. Delivered Image Quality

Figure 7 shows contour diagrams from an R-band image taken during excellent seeing conditions of 0.65" (2.5 pixels) at two points in the focal plane: one at the center and one at the extreme corner.

We can compare the true image in Figure 7 with the spot diagrams in Figure 8. The central image in Figure 7 is very round, with a slight ellipticity in the outer halo. The image from the field corner is more elliptical and diffuse. Figure 8 shows that the degradation of the image (e.g., in the R-band) expected is similar to that observed.

Tests of the ADC have been made under conditions of ~1" seeing. With the ADC set to its null position, and the telescope observing at 60°, ellipticity in the resulting images is evident. With the ADC prisms set to the appropriate angles, there is no evidence for residual ellipticity.

Detailed astrometric tests have been performed in the VRI bands and analyzed by Lindsey Davis. She finds that the plate scale is precisely as predicted: 17.43"/mm in VRI (center), and 16.39"/mm in VRI (corner, 0.42° out). These correspond to effective focal ratios of 3.14 at the center and 3.34 at the corner.

3.2. Using the ADC

The ADC is designed to provide optimum correction for a single passband at a time. It will not completely correct the full optical spectrum. This scheme provides better image quality for the specific passband, but adds some operational complexity as described below.

Modes of Operations: There are 3 modes in which the ADC system can be used.

1. Null mode, where the ADC prisms are set to a fixed position and make no correction for the atmosphere.
2. Track mode, where prism rotations are updated automatically, usually at 1 minute intervals. This mode accounts for the continuously changing zenith and azimuth angles of the telescope as it tracks an object or slews.

3. Preset mode, where the prism rotations are set at the beginning of an exposure to be correct for the middle of the exposure, but otherwise not moved. In this mode, the prisms do not move during an exposure to guard against any possible shifting of the images due to prism motions.

In practice, we have found that the telescope autoguider adequately compensates for the tiny motions when Track mode is used. Consequently, we suggest using Track mode to improve image quality with a minimum of attention to ADC operations.

ADC Filter Mode: In the Track and Preset modes, the positions of the prisms are dependent on the observing bandpass because the optimum corrections are wavelength dependent. Thus, in using the ADC, it is necessary to select the proper filter mode (essentially, the bandpass) in the ADC control panel on the computer. This operation will force the prism motions to follow the algorithms tuned optimally for the specific bandpass of the filter.

While it is not necessary to compensate for atmospheric dispersion when using narrow-band filters, the guide cameras have separate broad-band filters that will see the effects of atmospheric dispersion. Differential refraction between the guider and the science CCDs will change as a function of telescope position and will cause blurring for long exposures at high zenith distances if the ADC is set to Null Mode. In this case, one should select an ADC Filter Mode that encompasses both the narrow-band filter and the TV camera filter bandpasses and select Track or Preset modes.

The ADC Graphical User Interface (GUI): With the relatively complex corrector system, control of the ADC prisms and modes is selected through a graphical display showing the various options and the user's selections. Status of the ADC prisms (prism angles, telescope altitude and azimuth, latest time of prism motion, last time of prism re-index) also is displayed in the graphical window.

3.3. The ADC prism algorithms

The ADC algorithms were developed from the model for atmospheric refraction[8] incorporated into the Zemax™ optical design software package. Separate algorithms for each of the UBVRI astronomical passbands were made by optimizing the Risley prism dispersion angles as a function of zenith distance at discreet points and then fitting a parameterized function. This was verified in-situ at the Mayall 4m telescope for each band within the limits of the delivered seeing. Some small improvement to the algorithm parameters may be possible, but would require superb seeing conditions to measure those parameters accurately.

4. SPECIAL ISSUES

The new corrector presented a variety of issues that had not been encountered in prior optical developments at NOAO. The most serious problem that arose was the image of the telescope pupil at the focal plane. Other items of note include our development of special optical coatings, in part to relieve the severity of the ghost pupil, and a software effort to map the pincushion distortion in the focal plane and correct for it.

4.1. The ghost pupil

The image of the pupil is nearly invisible (less than a 1% effect) in images taken through broad-band filters. However, images taken through narrow-band interference filters reveal the ghost at levels that correlate inversely with the width of the filter bandpasss. That is, narrow filters introduce a strong ghost. The cause is somewhat subtle. Light passing through the corrector either passes through the narrow-band filter, or it is reflected back toward the primary if the light is outside the center of the filter bandpass. The rejected light encounters surface A of corrector element #4, and a fraction (<1%) of this light is reflected back once again to the detector, if it can make it through the filter on its second attempt. This time, though, the light is coming at the detector from a much wider range of angles since it is not being imaged by the primary, but rather, from the relatively nearby surface A of element #4. At these large angles, the acceptance bandpass of the interference filter becomes very wide and some light, originally outside the bandpass, makes it through to image on the detector. A typical ghost image is shown in Figure 9 before and after processing to remove the effect.

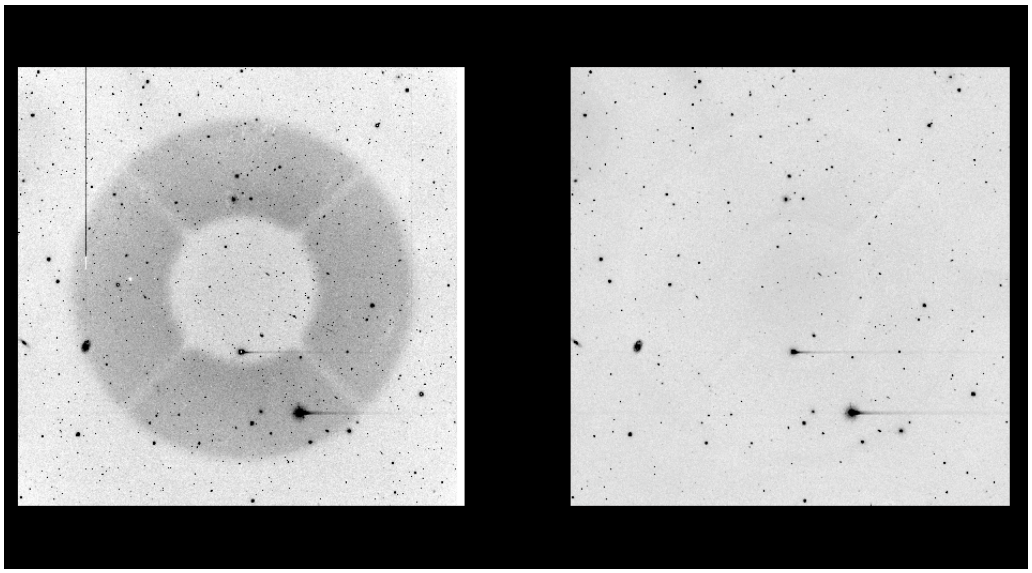

Figure 9. An image taken through a narrow-band filter (4.5 nm) of the central 14' X 14' field of the new corrector is shown. The ghost pupil is clearly evident in the left panel (at an amplitude of about 15%), but is almost undetectable in the right panel, which shows the image after processing with flat-field exposures. Normally, the ghost would have an amplitude of ~4%, but the Sol-Gel coating had deteriorated by the time this image was taken (see text).

Software removal of the interference-filter induced ghost image requires the following procedure. First, flat-field exposures of the sky are taken during twilight. The background sky level underlying the ghost pupil is subtracted. The remaining image of the pupil is then scaled to the magnitude of the ghost in the target image and subtracted. Usually, this process requires a few iterations to find the optimum scaling factor for best removal. The residual pupil image after subtraction is almost always less than 1%, and often about 0.25% of the background sky in the target image.

4.2. Optical coatings

Since the magnitude of the ghost pupil is directly proportional to the reflectivity of surface A of element #4, we investigated the possibility of applying an extremely low reflectance (high transmission) coating to this surface. Cleveland Crystals developed a process to apply Sol-Gel coatings that are tuned to a specific wavelength for excellent performance (~0.1% reflectivity), and also to provide very low reflectivity (~1.0%) over a very wide spectral region. When first applied, the ghost pupil amplitude was reduced to <4% with narrow-band filters and <1% with broad-band filters.

Unfortunately, the longevity of the Sol-Gel coating was compromised due to contaminants in its enclosed environment. The contamination is reversible, but this must be prevented from occurring again. We are working with the DAO and Cleveland Crystals to develop a process that provides a much longer lifetime for the Sol-Gel. The effect of the contamination is to increase the reflectivity and the amplitude of the ghost pupil in direct proportion (factor of ~3-4).

4.3. Distortions

As noted earlier, there is mild, nearly quadratic, pincushion distortion such that pixels in the corner of the Mosaic CCD see ~6% less sky (linearly along a radial vector) than do those pixels near the center of the array. This factor is slightly color-dependent, having values of 6.49%, 6.36%, and 6.29% for the U, V, and I bands. Because this is almost purely a radial factor, the area of a pixel changes less dramatically than the square of the distortion term, and is roughly an 8% factor in the corner of the array. Care must be taken when analyzing photometric data; Tod Lauer[9] discusses the issues in terms of applying the proper flat-field corrections for extended, versus point-source, objects.

4.4. Design improvements

If we were to build a new corrector again, we would certainly try to avoid the single biggest problem – the ghost pupil. In a new optical design, we would control the field lens (element #4) to eliminate the surface curved toward the detector. If that surface were required, the radius of both surfaces of the field lens would be made a little shorter or much longer to destroy the R=2*D condition, where R is the radius of the surface curved to the detector and D is the distance of this surface to the detector. Image quality may be degraded relative to the present design, though, with this added constraint. We note that ghost pupil images are common to these 4-element correctors, though not generally to the degree evidenced here.

We wish to thank Gary Muller for his design and engineering help in the corrector project, and for drafting the opto-mechanical layout figures for this paper (Figures 2 and 5). Dick Sumner was responsible for the superb quality of the optical elements in the corrector. Dr. Lindsey Davis performed the on-sky astrometric analysis to verify that the predicted and actual plate scales were identical, and provided the software to remove the distortions. David Mills and Shelby Gott provided the software to control and report status of the ADCprisms. GHJ wishes to thank Peter Strittmatter for providing a sabbatical office at Steward Observatory during the period when this paper was written.

6. REFERENCES

1. C. G. Wynne, “Ritchey Chrétian Telescopes and Extended Field Systems”, *Ap. J.*, **152**, pp. 675-694, 1968.
2. G. P. Muller, R. Reed, T. Armandroff, T. Boroson, G. Jacoby, “What is Better than an 8192 X 8192 CCD Mosaic Imager?”, SPIE Conference 3355, this volume.
3. T. E. Ingerson, “Empirical and Theoretical Modeling of the PFADC Corrector on the Blanco 4m Telescope”, PASP submitted, March 1998.
4. P. R. Yoder, Opto-Mechanical Systems Design, pp. 145-153, Marcel-Dekker, New York, 1986.
5. M. Bayar, “Lens Barrel Opto-Mechanical Design Principles”, *Optical Engineering*, **20**, no. 2, p. 185, 1981.
6. Ibid., p.182.
7. D. Vaughnn, “Electrostatic Application of Black Flocking for Reducing Grazing Incidence Reflections”, in Optical System Contamination V and Stray Light and System Optimization, A. Peter M. Glassford, Robert P. Breault, Stephen M. Pompea, Editors, Proc. SPIE 2854, pp 416-428 (1996).
8. P. K. Seidelmann, Ed., "Refraction - Numerical Integration", Section 3.281, Explanatory Supplement to the Astronomical Almanac, pp. 141-143, University Science Books, Mill Valley, 1992.
9. T. Armandroff et al., “NOAO CCD Mosaic Imager User Manual”, http://www.noao.edu/kpno/manuals/mosaic_man.html, pp. 42-43, 1997